2

SAND-93-1874C
CONF-931191--3

Fluorescent Microthermographic Imaging

Daniel L. Barton

Electronics Quality/ Reliability Center
Sandia National Laboratories
Albuquerque, NM 87185
Phone: (505)844-7085
FAX: (505)844-2991
E-mail: BARTONDL@mdlchtm.eece.unm.edu

Introduction

The need for a technique that would produce high spatial and thermal resolution images of microelectronic devices has been around for many years. In the early days of microelectronics, design rules and feature sizes were large enough that sub-micron spatial resolution was not needed. Infrared or IR thermal techniques were available that calculated the object's temperature from infrared emission. As will be shown in this tutorial, there is a fundamental spatial resolution limitation dependent on the wavelengths of light being used in the image formation process. As the integrated circuit feature sizes began to shrink toward the one micron level in the early 1980's, the limitations imposed on IR thermal systems became more pronounced. Something else was needed to overcome this limitation. Liquid crystals have been used with great success, but they lack the temperature measurement capabilities of other techniques. Liquid crystals provide a binary response, indicating if the hot area is above the crystal's transition temperature or not [1-3].

The fluorescent microthermographic imaging technique (FMI) was developed to meet this need [4,5]. This technique offers better than 0.01 °C temperature resolution and is diffraction limited to 0.3 μm spatial resolution. While the temperature resolution is comparable to that available on IR systems, the spatial resolution is much better. The FMI technique provides better spatial resolution by using a temperature dependent fluorescent film that emits light at 612 nm instead of the 1.5 μm to 12 μm range used by IR techniques.

This tutorial starts with a review of blackbody radiation physics, the process by which all heated objects emit radiation to their surroundings, in order to understand the sources of information that are available to characterize an object's surface temperature. The processes used in infrared thermal imaging are then detailed to point out the limitations of the technique but also to contrast it with the FMI process. The FMI technique is then described in detail, starting with the fluorescent film physics and ending with a series of examples of past applications of FMI.

Blackbody radiation - Basic Physics [6]

It is well known that heated objects emit radiation. Most of us have observed a red hot heating element on a stove or have looked at a red hot poker that has been withdrawn from a fire. Items such as these appear hot to us not because we felt the heat, but because we could see the radiation emitted by the object. As objects are heated beyond the red hot temperature, approximately 700 °C, the amount of radiation being emitted in the visible range increases and the objects begin to turn orange, then yellow, and eventually to a bluish-white color. For example, the sun has a surface temperature of 5700 K and gives off a visible light with a peak around 510 nm. The North Star, by comparison, has a surface temperature of 8300 K and gives off radiation peaked at 350 nm. What is not readily apparent to us is that most of the light being emitted by hot objects is infrared. As natural evolution would have it, our eyes have developed so that their spectral response is well suited to the peak wavelengths being emitted by our sun. The spectral sensitivity of the human eye is shown in Fig. 1.

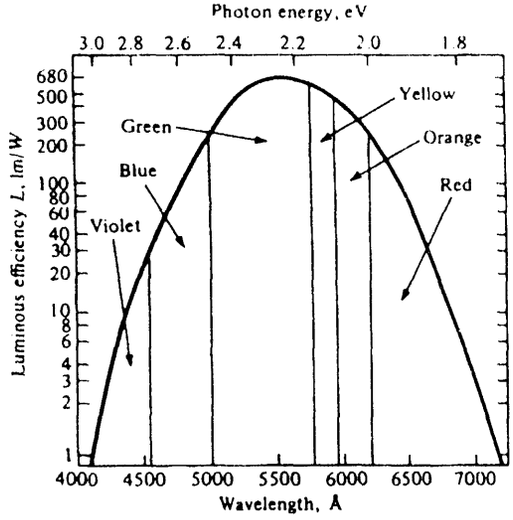

Fig. 1 - Spectral response of the human eye [7]

The connection between the peak radiation wavelength and temperature forms the basis for infrared (IR) temperature measurement. Physicists in the late 19th century knew the relationship between the temperature of a blackbody, a body that absorbs all of the radiation incident upon it, and the peak wavelength of the radiation being given off by that body, but could not describe that relationship mathematically. The most important observation was that all blackbodies at the same temperature emitted radiation with the same spectral distribution, regardless of their composition. The spectral distribution of the radiation emitted by a blackbody is known as the spectral radiancy, $R_T(\nu)$, where ν is the frequency of the radiation. The quantity $R_T(\nu)$ is defined so that $R_T(\nu)d\nu$ is the energy emitted per unit time in the frequency range ν to $\nu + d\nu$ from a unit area on a surface at temperature T. Example spectral radiances of blackbodies at temperatures ranging from 1000 K to 2000 K are shown in Fig. 2.

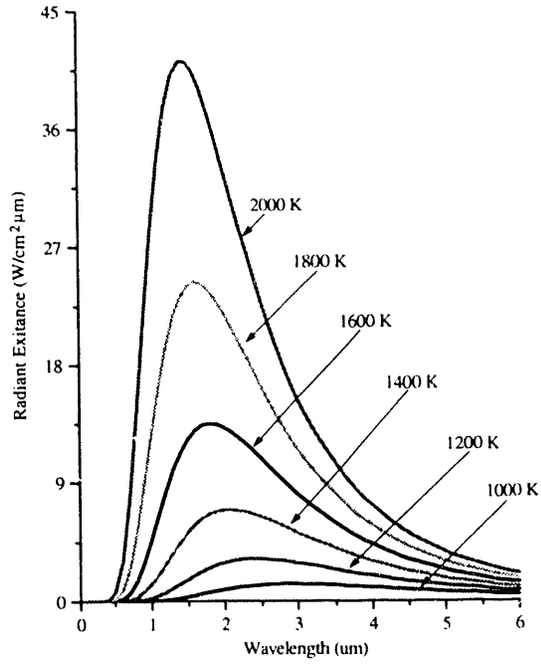

Fig. 2 - Spectral radiance of blackbodies at 1000 K to 2000 K

The data plotted in this figure has been plotted as a function of wavelength instead of frequency as is described above. The integral of the spectral radiancy $R_T(\nu)$ over all frequencies is known as the radiancy, R_T, or

$$R_T = \int_0^\infty R_T(\nu)d\nu.$$

In Fig. 2, it is evident that the radiancy increases with increasing temperature of the body. The relationship between the radiancy and temperature was first formulated in 1897 and is known as Stefan's Law,

$$R(T) = \sigma T^4.$$

Though Stefan's Law was defined empirically in its original form, the constant σ came to be known as the Stefan-Boltzmann constant with a value of

$$\sigma = 5.67 \times 10^{-8} \frac{W}{m^2 \cdot K^4}.$$

Also evident from Fig. 2 is the relationship between the wavelength of maximum spectral radiance and temperature. It is evident that the peak wavelength decreases with increasing

temperature. The relationship between wavelength peak and temperature is known as Wein's displacement law, which can be written,

$$\lambda_{MAX} = \frac{2.898 \cdot 10^{-3}}{T}$$

where T is the temperature in degrees Kelvin. The result of the equation is λ_{MAX} in meters.

Classically, if we consider a small hole in a cavity as an approximation of a blackbody, (this happens to be a very good blackbody), we can easily find the number of modes present in the cavity and assign an energy to each of these modes which should describe blackbody radiation. If we realize that the spectral radiancy of a blackbody is directly proportional to that of a cavity,

$$\rho(\nu) \propto R(\nu)$$

and use the equapartition of energy theory where each mode of the cavity is assigned an energy, $\bar{\varepsilon} = kT$, we end up with the Rayleigh-Jeans formula for blackbody radiation

$$\rho_T(\nu)d\nu = \frac{8\pi\nu^2 kT}{c^2} d\nu.$$

This formula proved to be accurate at low frequencies, but failed miserably at high frequencies in the ultraviolet end of the spectrum. This theory was ultimately known as the ultraviolet catastrophe. The reason for the failure of this theory is simple. The equapartition theorem is only valid for a continuous distribution of energies. However, the energy of an electromagnetic wave is quantized in units of hν. The theory of energy quantization led Max Planck to the correct equation to describe the blackbody radiation spectrum

$$\rho_T(\nu)d\nu = \frac{8\pi\nu^2}{c^3} \cdot \frac{h\nu}{e^{\frac{h\nu}{kT}} - 1}.$$

In most applications, the object under examination will not be a perfect blackbody. As such, the radiancy will have to be corrected for the emissivity of the material. The emissivity, e, is defined through Stephan's Law which relates the radiancy to temperature,

$$R(T) = e \cdot \sigma T^4$$

By definition, the emissivity of a material is the ratio of the energy radiated by a given object to the energy radiated by a blackbody at the same temperature. The emissivities of

many materials have been measured and are generally available. Table 1 lists several common materials and their emissivity values.

Now that the theory of radiation from heated objects has been reviewed, we are ready to understand the emission spectrum of objects encountered in the microelectronics industry. Returning again to Fig. 2, we see that even for objects at 2000 K, there is only a small portion of the radiated energy in the visible portion of the spectrum. In fact, the majority of the information relating to the object's temperature is well into the infrared region of the electromagnetic spectrum. In the semiconductor industry, there are few devices that operate at such high temperatures. If we expand the scale shown in Fig. 2 to temperatures around room temperature, we begin to understand the difficulties in performing high spatial resolution thermal imaging on semiconductor devices. Fig. 3 shows blackbody radiation spectra for objects between 250 K and 350 K. Of particular interest in this figure is the curve for 300 K. It is clear from this curve, that very little energy is emitted at wavelengths less than about 3 μm and most of the energy is emitted at wavelengths greater than 5 μm. In order to collect the infrared radiation information from objects near room temperature, a detector sensitive well into the infrared range is needed.

Table 1 - Emissivity of various materials [8,9]

Material	Emissivity
Ideal black body	1.0
Lampblack	.95
Asbestos paper	.95
White Lacquer	.95
Bronze paint	.8
Carbon, rough plate	.76
Oxidized steel	.7
Polished brass, oxidized copper	.60
Aluminum paint	.55
Oxidized monel metal	.43
Cast iron - polished	.25
Copper - polished	.15
Nickel - polished	.12
Aluminum - highly polished	.08
Platinum - highly polished	.05
Silver - highly polished	.02

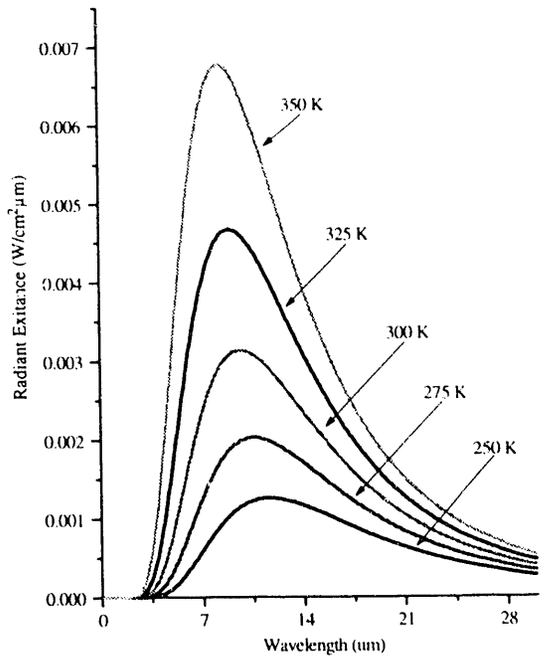

Fig. 3 - Spectral radiance of blackbodies at 250 K to 350 K

Infrared (IR) Thermography [8-12]

It is evident from Fig. 3 that to use the physics presented in the previous section on semiconductor devices we must analyze the radiation emitted by the sample in the 3 μm to 12 μm range. Most commercially available IR thermography systems use one of two types of detectors; indium antimonide or mercury cadmium telluride. Indium antimonide (InSb) detectors are sensitive in the wavelength range 1.5 μm to 5.5 μm. Mercury cadmium telluride (HgCdTe) detectors are sensitive over the range of 8 μm to 12 μm. Both detectors offer similar temperature sensitivities and ranges, but InSb operates at shorter wavelengths and should have somewhat better spatial resolution. Table 2 lists several manufacturers of IR thermography equipment and their performance characteristics.

The data in Table 2 shows that, while IR thermal imaging systems have excellent potential for temperature resolution, they suffer from a fundamental limitation on spatial resolution. In general, the spatial resolution of a microscope is limited by the wavelength of light. The relationship between resolution and wavelength as given by Lord Rayleigh's criteria can be written [13]

$$\text{Resolution} = \frac{0.61 \cdot \lambda}{\text{N.A.}}$$

Table 2 - Thermography equipment for semiconductor and hybrid production applications [14]

Company/Models	Detector (std/opt)	Max. IR spectral range in μm (std/opt)	Temperature range (low/high °C)	Temperature resolution (°C/@°C)	Spatial[1] resolution
AGEMA IR Thermovision 782LWB	InSb/ HgCdTe	2-5.6 8-12	-20/1600	0.1/30	15 μm
Barnes Engineering					
Computherm	InSb	1.5-5.5	amb/600	0.1/75	15 μm**
RM-2A Microscope	InSb	1.5-5.5	amb/500	0.1/75	8 μm
Hughes	InSb/	2-5.6			
Probeye Series 4000	HgCdTe	8-12	-40/1500	0.1/22	2.2 mrad
Inframetrics					
Model 600	HgCdTe	3-12	-20/1500	0.1/30	30 μm
Mikron Instrument	HgCdTe/	8-13/			
Thermo Tracer 6T61	InSb	1.5-5.5	-50/2000	0.1/70	100 μm
UTI					
CCT-9000	HgCdTe	8-14	-50/350	0.1/75	600 e/l

notes:
std = standard
opt = optional
amb = ambient
e/l = elements per line
1. Spatial resolution using microscope objective
** Their latest system quotes 4 μm spatial resolution

where λ is the wavelength of light being imaged and N.A. is the numerical aperture of the microscope. This result although very simple, provides a good estimate of the resolving power of a microscope system. In Lord Rayleigh's own words, "*The rule is convenient on account of its simplicity and it is sufficiently accurate in view of the necessary uncertainty as to what is meant by resolution.*" [13]

This relation clearly shows that IR thermal systems that gather radiation in the 1.5 μm to 12 μm range will not be able to resolve sub micron structures that are found on modern VLSI integrated circuit technologies. Before discussing how to circumvent this limitation, we should review the general theory of operation of IR thermal systems.

In general, there are several ways to measure the temperature of an object. The simplest method is measure the radiance and, if the emissivity of the material is known, directly compute the temperature of the sample. Systems of this type use a very simple photovoltaic type detector that is sensitive in the IR wavelengths. Cooled InSb photovoltaics are perhaps the most common. These detectors are generally sensitive in the 1.5 μm to 5.5 μm range. An example is the Barnes RM-2A infrared radiometric microscope [8].

To directly measure the temperature of a sample, the radiance is measured first. The radiance from a sample at a given temperature is related to the radiance from a blackbody at the same temperature by the emissivity, or

$$R_T = e \cdot R_{TBB}$$

where R_T is the radiance from the sample, e is the sample's emissivity, and R_{TBB} is the radiance of a blackbody at the same temperature. Ideally, if the sample's emissivity is known, its temperature can be calculated if the relationship between the radiance collected by a given system from a blackbody and its temperature is known.

In order to increase the accuracy of the temperature measurement, the radiance that is reflected by the sample must be accounted for. Thus, the total radiance collected by a system from a sample would be

$$R_{Total} = R_T + (1-e)R_0$$

where R_0 is the radiance emitted by the ambient background. Combining the last two equations, the total radiance collected by the system is

$$R_{Total} = e \cdot R_{TBB} + (1-e)R_0.$$

If the emissivity is known and the ambient radiance can be accounted for, the temperature of the sample can be found.

Lastly, the spectral response of the system must be considered. In general, the system response will not be flat over the range on interest. The introduction of an "effective" blackbody radiance representing a convolution of the blackbody radiation spectrum and the IR microscope/detector response must be known. This information has usually been characterized by the manufacturer and is incorporated into their blackbody radiance to temperature conversion algorithm.

If the emissivity of the sample is not known, a comparison between the radiance measured from the unknown at a known temperature and from a blackbody can be performed. While measurements of this type can be easily done on uniform macroscopic samples, making these measurements on VLSI integrated circuits is difficult, but not impossible.

More elaborate IR imaging systems have been developed which scan the sample and create a two-dimensional image of the surface radiance [9]. Non-scanning systems simply add up the radiance from the entire field of view, or a pre-selected portion of it, and convert that radiance to temperature. Scanning systems allow surface temperature measurements to be made on samples with multiple areas of different emissivity values in the field of view. While the theory of operation is as before, calibration of the system requires that the user measure the radiance of the sample at two known temperatures using a sample stage heating unit. This measurement allows for the creation of an emissivity map of the sample surface over the temperature range of interest.

Fluorescent Microthermographic Imaging

History

The concept of using a film with a temperature dependent fluorescence quantum yield to generate high resolution thermal maps of integrated circuits was first published in 1982 by Paul Kolodner and J. Anthony Tyson at Bell Laboratories [4]. Their first work described a technique which could yield thermal images with a thermal resolution of 0.006 °C and a spatial resolution which was equipment limited to 15 μm. They noted that spatial resolutions of better than 1 μm were achievable with different optics and a better camera . This improvement in spatial resolution was demonstrated less than a year later in the second work published by the same authors [5]. The goal of this second work was to demonstrate the spatial resolution capability of the technique, which they measured to be 0.7 μm.

In the following years, a company called Lassen Research was licensed by Bell Laboratories to market turn-key fluorescent microthermography systems based on the work of Kolodner and Tyson. To the author's knowledge, only a handful of systems were sold, all within the AT&T system. This author's experience with FMI is with one of these systems and with subsequent development of a system to exploit this technology to its limit.

Word of the usefulness of FMI has spread throughout the failure analysis field and now at least a half-dozen failure analysis engineers are developing systems on their own for their companies. The recent interest in FMI has caught the manufacturer of the fluorescing film, Eastman Kodak, by surprise. Since the compound of choice has not been used widely, the supply at the manufacturer was small. The renewed interest in the technique will hopefully be enough that supply problems do not deter interested engineers from using FMI in their laboratories.

This tutorial will lead readers through the theory behind the technique, describe the hardware and image processing requirements needed, and discuss some example applications. The preceding sections on blackbody radiation and IR thermography were included so that the readers can understand thermal imaging concepts, the nature of the signals that are present, and why there is a fundamental limitation on spatial resolution imposed by using imaging IR radiation. While IR thermography is invaluable to the microelectronics industry, its applications are limited when the areas of interest are sometimes an order of magnitude smaller then the available spatial resolution. Applications such as these are where FMI is unchallenged.

EuTTA Compound Specifics: [15-18]

During the late 1950's and early 1960's, there was a great deal of laser research. Some of this work dealt with the use of rare earth chelates as sources for use in liquid lasers. Rare earth chelates were identified as possible sources because of their well known fluorescence responses to UV or near-UV excitation sources. One of these compounds, EuTTA (europium thenoyltrifluoroacteonate) is the focal point for the fluorescent microthermal technique. The availability of compounds such as EuTTA is the main reason that the fundamental limitation on spatial resolution encountered in IR thermal systems could be overcome.

EuTTA is not the only compound available for FMI. In fact, there are chelates of all of the rare earth elements which include La, Sm, Eu, Gd, Tb, Dy, Tm, Yb, and Lu. The europium system was ultimately selected by the developers of FMI as the most suitable because of its temperature characteristics, emission/absorption characteristics, availability, and other qualities. There are several other europium compounds which might be suitable for FMI. Other β–diketone chelates of europium are available such as europium benzoylacetonate, europium dibenzoylmethide, and europium hexfluoroacetonate in addition to EuTTA. EuTTA however, has the best fit for temperature dependent fluorescence quantum yield in the temperature range near room temperature.

To better understand the theory behind FMI, we need to discuss the process which gives the fluorescing film a temperature dependent fluorescence quantum yield. Fig. 4 shows the molar excitation coefficient (or loosely, the absorption spectra) versus wavelength for EuTTA. These were measured for EuTTA in an ethanol solution. While FMI requires that EuTTA be suspended in a solid matrix, the data in Fig. 4 indicates the excitation wavelengths of interest. First, there is a broad absorption peak centered around 335 nm. This is where the TTA ligand absorbs energy. After about 360 nm, the amount of incident radiation that is absorbed falls off strongly. The two peaks at 460 nm and 525 nm are consistent with Eu^{3+} levels and are not of interest from an excitation viewpoint. What is of interest is the lack of absorption for wavelengths much above 500 nm. This allows for a strong separation between the excitation source and the fluorescence emission.

The ultraviolet radiation used to excite the EuTTA fluorescence does so through an intermolecular energy transfer. The TTA ligand absorbs the UV light then transfers the energy to the europium ion. While several fluorescence lines are excited, the transition from the Eu^{3+} $^5D_0$ energy level to the $^7F_2$ level is the most efficient. This transition generates the bright fluorescence line at 612 nm which is used for FMI. Fig. 5 shows the emission spectrum for crystalline EuTTA at 25 °C.

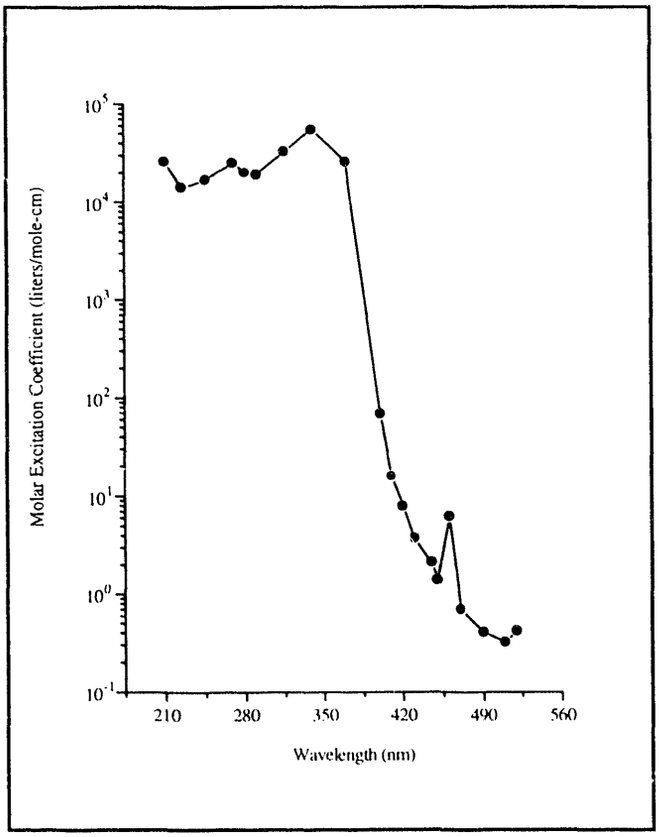

Fig. 4 - Absorption spectra for EuTTA (in solution) [15]

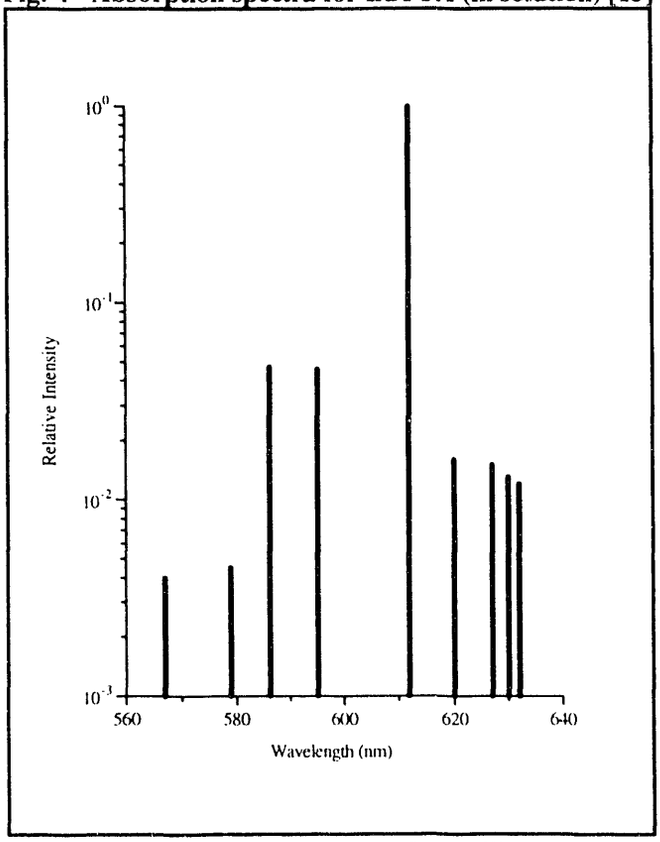

Fig. 5 - Emission spectra of EuTTA (Crystalline) at 25 °C [15]

For thermal imaging applications, we need to know how the emission spectra of the compound changes with temperature. The temperature dependence of this europium chelate was considered a problem for liquid laser applications, but it is what FMI relies upon for image formation. Fig. 6 shows the measured absolute quantum yield versus temperature and Fig. 7 shows the decay time of the fluorescence yield versus temperature. Both of these plots were generated for EuTTA in an ether:isopentane:ethanol (5:5:2) solution. For the FMI application, a curve will need to be generated for each compound mixture that is used. These data have been included to illustrate the temperature dependence of EuTTA.

The fit curve in Fig. 6 was plotted using the equation

$$Q(T) = 0.398 - 0.07 \cdot e^{0.031 \cdot T}$$

where Q(T) represents the quantum efficiency of the compound. The behavior of this compound over this broad temperature range is very predictable and provides a simple way to calculate the temperature of an object by imaging its change in quantum yield.

The information in Figs. 6 and 7 illustrates the intermolecular energy transfer between the TTA ligand and the europium ion. First, notice that the quantum efficiency falls off faster than the decay time with increasing temperature. This shows that we may have a low quantum efficiency even at low temperatures due to a loss of excitation energy of the Eu^{3+} ion. The change in quantum efficiency with temperature is an indicator of the quenching of the whole system, while the fluorescence decay time is an indication of quenching of the fluorescence in the europium ion itself.

The standard application technique for using EuTTA for FMI is to incorporate the chelate into a PMMA (polymethylmethacrylate) matrix. A typical starting point is a solution consisting of 1.2 wt% EuTTA, 1.8 wt% PMMA, and 97 wt% MEK (methylethylketone). The MEK is a very high vapor pressure solvent that evaporates rapidly leaving the EuTTA/PMMA mixture on the sample [4]. Typically this mixture is spun on the sample and allowed to cure in an oven at 125 °C for about 30 minutes. Ideally, the film should only be several optical absorption lengths thick. At an excitation wavelength of 365 nm, a 300 nm film is approximately 3.5 optical absorption lengths thick. The idea is to have the film thick enough that most of the UV light is absorbed, but thin enough that the thermal profile of the sample surface is not distorted. As we will find out in later sections, the image processing required to create a thermal image reduces the influence of film non-uniformity on image quality. As such, the film should be as uniform as possible, but great pains to achieve perfect uniformity of film composition and thickness are not necessary.

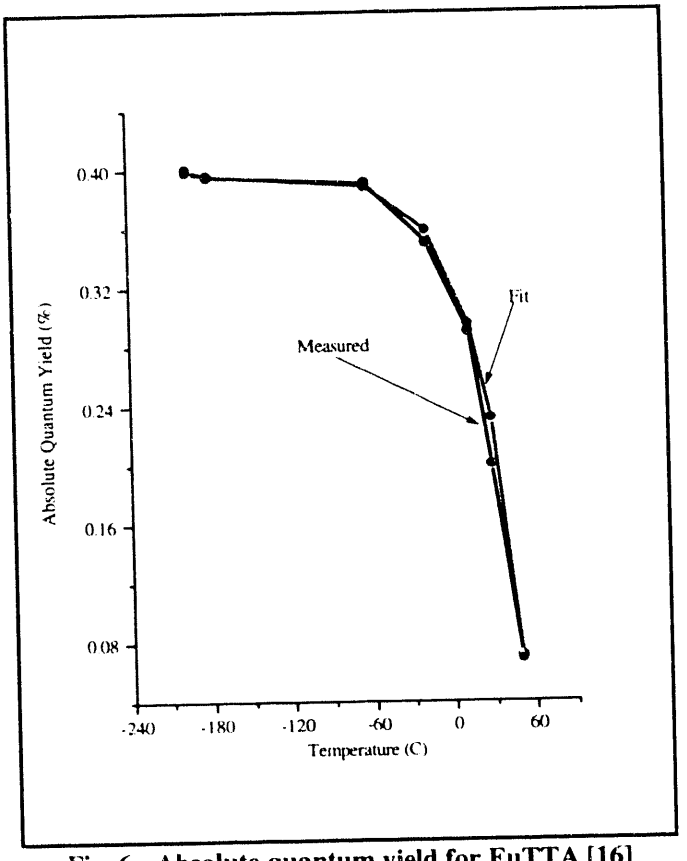

Fig. 6 - Absolute quantum yield for EuTTA [16]

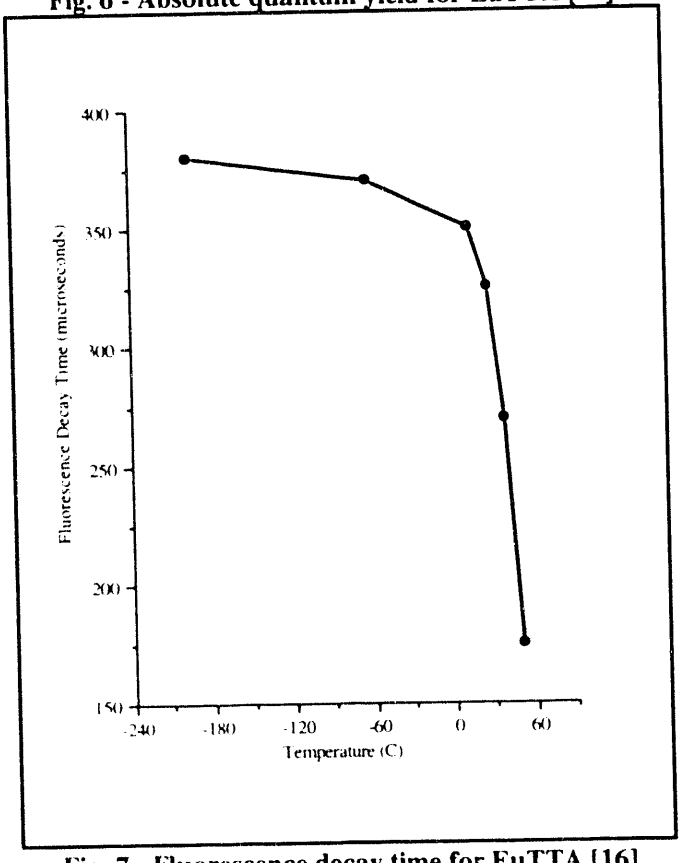

Fig. 7 - Fluorescence decay time for EuTTA [16]

The EuTTA/PMMA composition can be varied as needed for any specific application. Adjusting the EuTTA content will change the amount of fluorescent light emitted from the coated sample and changing the amount of MEK in the mixture will thin the solution out for applications where spinning the sample is not practical. For instance, integrated circuits in packages are sometimes difficult to mount on a photoresist spinner. The use of a thinned out mixture would allow a thin film to be deposited without spinning the IC. Usually, spinning a packaged IC will cause the mixture to accumulate around the ball bonds leaving a thick film in these areas. The thick film is often not a problem, unless the input structures are the areas of interest. For these applications, a thinner mixture or a higher spin rate would be in order.

The advantage of PMMA is that it can easily be removed once the thermal analysis is completed. Rinsing the sample in acetone will dissolve the film in several minutes. The use of other polymers such dPMMA, (perduetero-poly-methylmethacrylate) will provide a stronger temperature dependence, but the additional cost of dPMMA is not justified. Other matrixes, such as Owens-Corning GR650 spin-on glass have been successfully used, but make film removal more difficult.

Regardless of the film type used, accurate absolute temperature measurements are possible but, because of the differences in the logarithmic slope of the quantum efficiency versus temperature curves for different materials, an accurate film calibration should be done for each type of premixed solution. The calibration curve can be easily obtained by using a hot/cold stage, a calibrated thermocouple, and the camera to be used for FMI. Simply record the total emission observed by the camera in a given time period with the sample at a given temperature. Varying the hot/cold stage temperature over as large a range as possible will give the best results. Samples such as blank wafers would be good for this process since, during the measurements, they will be close to the hot chuck temperature. The emission versus temperature data can easily be plotted and a logarithmic slope can be found. Unless the composition of the mixture changes drastically, this measured slope need only be done once, especially if only relative temperature measurements are needed.

For higher temperature measurements, another europium compound, perduetero-(tris-6,6,7,7,8,8,8-heptafluoro-2,2-dimethyl-3,5-octandionato) europium (dEuFOD) may be used up to about 200 °C. dEuFOD has a much weaker temperature dependence both for fluorescence quantum yield and fluorescence lifetime than EuTTA [19].

A general consideration when working with rare earth elements is their inherent toxicity. The MSDS for EuTTA has been included in Appendix A for reference. Section IV of this MSDS lists the toxicity and health hazard data. Sections A and B indicate that the toxicological effects of this material have not yet been established. Always be sure to take proper precautions when handling EuTTA.

Image Processing:

Now that we have an understanding of the fluorescent film properties which allow us to use this technique to generate thermal images, we need to cover how that information is converted to temperature data. Returning to Fig. 6, we recall that the quantum efficiency versus temperature can be represented as an exponential. Fitting an exponential function to the data in Fig. 6 gave us,

$$Q(T) = 0.398 - 0.07 \cdot e^{0.031 \cdot T}$$

as the quantum efficiency versus temperature relationship. The light intensity at a given point, (x,y), on the image can be represented by

$$S(x,y) = I(x,y) \cdot \eta(x,y) \cdot r(x,y) \cdot Q(T(x,y))$$

where I(x,y) is the illumination intensity, $\eta(x,y)$ is the optical collection efficiency, r(x,y) is the sample reflectivity, and Q(T(x,y)) is the quantum efficiency. In order to remove all spatial artifacts included in the I, η, and r terms, and leave an image containing only thermal information, we can divide an image taken with the sample under bias, i.e. a hot image, by one without bias, i.e. a cold image. The result is a map of the ratio of quantum efficiencies between hot and cold images

$$S_R(x,y) = \frac{S_H(x,y)}{S_C(x,y)} = \frac{I(x,y) \cdot \eta(x,y) \cdot r(x,y) \cdot Q(T_H(x,y))}{I(x,y) \cdot \eta(x,y) \cdot r(x,y) \cdot Q(T_C(x,y))} = \frac{Q(T_H(x,y))}{Q(T_C(x,y))}.$$

If we were working with a pure exponential, this ratio would be directly proportional to the difference in temperature, T_H-T_C. The problem with doing this directly is the 0.398 constant in the fit for Q(T) given above.

Once way around this problem is to create a carefully measured calibration curve for a given film mixture, using a given illumination intensity, on a given optical setup, etc. and use that curve as Q(T) above. This method allows accurate *absolute* temperature measurements to be made, but adds a great deal of difficulty to the FMI process. Problems with this process arise from small changes in equipment creating changes in light collection from a sample at a given temperature. For example, since the fluorescence intensity *decreases* as the film gets hotter and the film degrades under exposure to UV light, the sample will appear hotter after repeated imaging sequences. The degradation will require repeated removal and re-application of the film for accurate results.

Since in most applications, relative rather than absolute temperature measurements are needed, the image math can be simplified greatly with only a slight loss in accuracy. We need to stress that the slight accuracy change does not decrease the sensitivity, or the smallest change in temperature that can be resolved, of the technique.

To modify the process to allow for relative temperature changes, continue with the equation for the ratio of quantum efficiencies that we had before, take the natural logarithm, and plot the result for temperatures around room temperature. This gives us,

$$\ln(S_R(T)) = \ln\left[\frac{Q(T_H)}{Q(T_C)}\right] \propto \delta T .$$

This equation is plotted in Fig. 8 with the cold temperature, T_C, set at 28 °C.

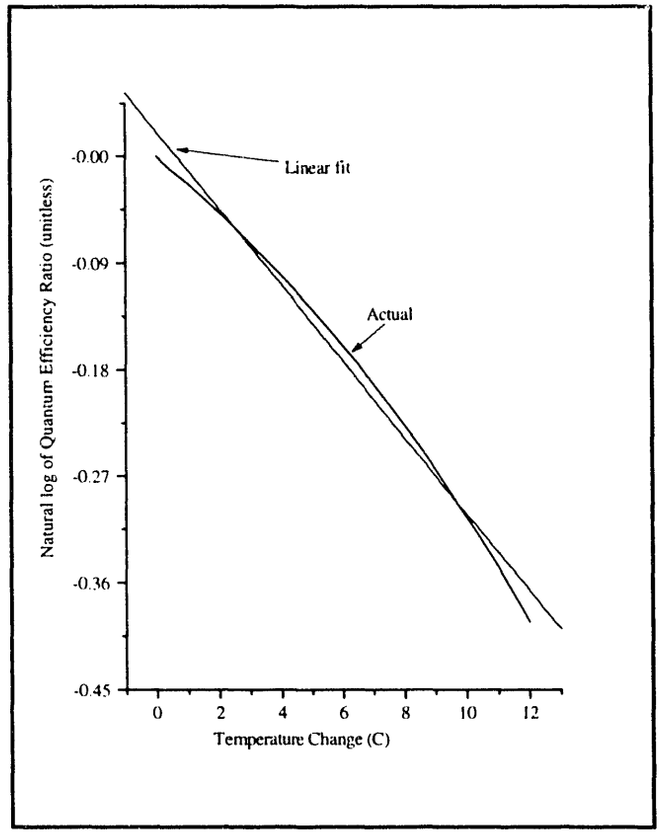

Fig. 8, Plot of quantum efficiency ratio around room temperature

The linear fit in Fig. 8 can be represented by the equation,

$$y = 0.02132 - 0.03233 \cdot x .$$

The standard deviation in the slope is 0.0006909, or less than one percent. The slope of the linear fit is what we need for temperature conversion. Once we have the slope, the rest is easy. Simply divide the natural log of the quantum efficiency relation by the slope. The result is the relative temperature change of a given pixel location.

$$\delta T \approx \alpha^{-1} \cdot \ln\left[\frac{Q(T_H)}{Q(T_C)}\right] = \alpha^{-1} \cdot \ln\left[\frac{S_H(x,y)}{S_C(x,y)}\right].$$

By simply taking the natural log of the ratio of the light intensities from a hot and cold image, we can divide the result by a constant and have a relative temperature measurement. This is the method presented in the literature [4,5] for use in FMI.

The examples that have been used here are based on the quantum efficiency versus temperature from EuTTA in solution, as described in the previous section. For EuTTA combined in a polymer or glass matrix, the fluorescence quantum efficiency will have the same temperature dependence, as this is dictated by the intermolecular energy transfer process, but they will be different. Published values for the slope of the linear fit in Fig. 8 for EuTTA in a dPMMA matrix are approximately -0.047 /°C [5]. This number will be different for EuTTA in PMMA or GR650 glass, as well as for EuFOD in dPMMA. Whatever chemistry is chosen, a calibration curve as outlined above must be made.

As an example, if a camera with 16-bit gray scale resolution is used and assuming the published value of the logarithmic slope of -0.047 /°C, the best possible thermal resolution would be:

$$\delta T \approx -0.047 \cdot \ln\left(\frac{65534}{65535}\right) = 0.324 \times 10^{-3} \mathrm{C}.$$

Comparing this with an 8-bit gray scale camera:

$$\delta T \approx -0.047 \cdot \ln\left(\frac{254}{255}\right) = 83.6 \times 10^{-3} \mathrm{C}.$$

This result will be referred to in the next section where hardware requirements are discussed.

Standard techniques can be used to reduce noise in the resulting thermal image. Image averaging on both the hot and cold images can be done prior to processing. Various techniques can be used after processing to enhance the thermal artifacts.

System Hardware:

There are essentially three main system components that are required for FMI. These components include a light source, a camera system, and an optical platform. This section discusses each of these areas and indicates differences between each of the possible choices.

The light source used for fluorescence excitation has the most possible choices. The absorption spectra for EuTTA (Fig. 4) indicates that we are interested in ultraviolet sources in the approximate range of 210 nm to 365 nm. Sources with wavelengths much greater than about 365 nm will require higher intensities to excite the fluorescence and thus are not practical. UV sources always present a hazard to the human eye so the use of proper eye protection is mandatory.

Most of the FMI systems currently in operation use arc lamps as their excitation sources. The most common lamps for UV applications are mercury, xenon, and mercury/xenon types. Examples of spectra for these types of arc lamps are shown in Fig. 9 and Fig. 10. It is clear from these figures that any of the three types of lamps suit the application well. Mercury bulbs have well known spectral peaks in the UV range and several that extend into the visible range. Xenon lamps have peaks in the upper end of the visible range, but have a broad continuum of output that extends usefully into the UV. Mercury/Xenon lamps combine the two spectra to create a broad range general purpose light source.

Arc lamps have been manufactured for many years. As such, one may be in storage somewhere in an old laboratory. While this old lamp may be good for demonstrating the FMI technique, modern arc lamps have benefited from years of research and are more stable sources. Stability of the light source, as evident from the last section, is one of the limiting factors in creating high temperature resolution images. If you decide to use an arc lamp as an excitation source, inquire about the stability of the light output as a key factor toward deciding which unit to purchase.

The other obvious choice for excitation source is a laser. Lasers differ from arc lamps in that all of their optical energy is in one narrow wavelength band rather than being spread over a continuum. Lasers are more efficient since all of the light output is within the wavelength range of interest. Table 3 lists some of the different laser systems and their respective lines. About half of the systems are listed as CW, or continuous wave, systems. These lasers have a continuous light emission. The remaining systems are pulsed, meaning they cannot sustain continuous emission and emit light in short pulses, usually with repetition rates up to several kilohertz. The choice between laser systems is usually cost. Many of the CW systems listed are very large laser systems, such as Argon Ion lasers, that have a weak line suitable for FMI. The problem is that you may have of purchase a laser with an output of several watts to yield several milliwatts for the UV line you need.

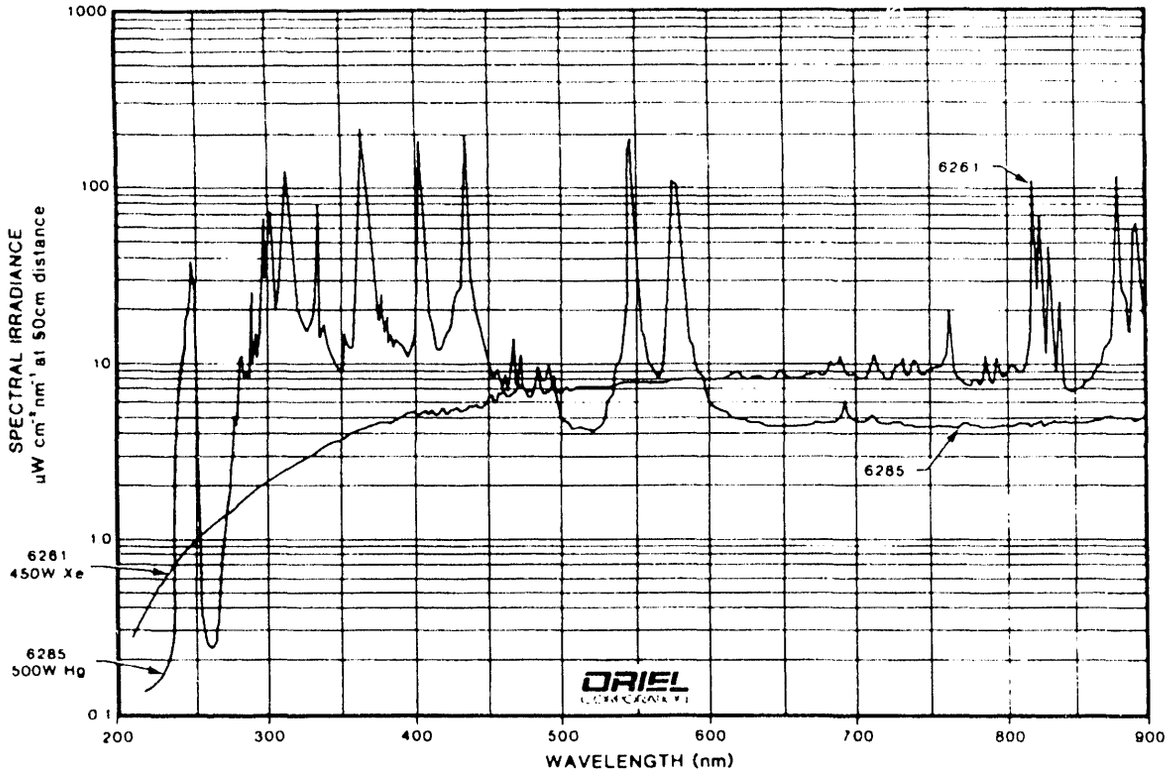

Fig. 9 - Spectral Irradiance of Xe (Xenon) and Hg (Mercury) arc lamps [20]

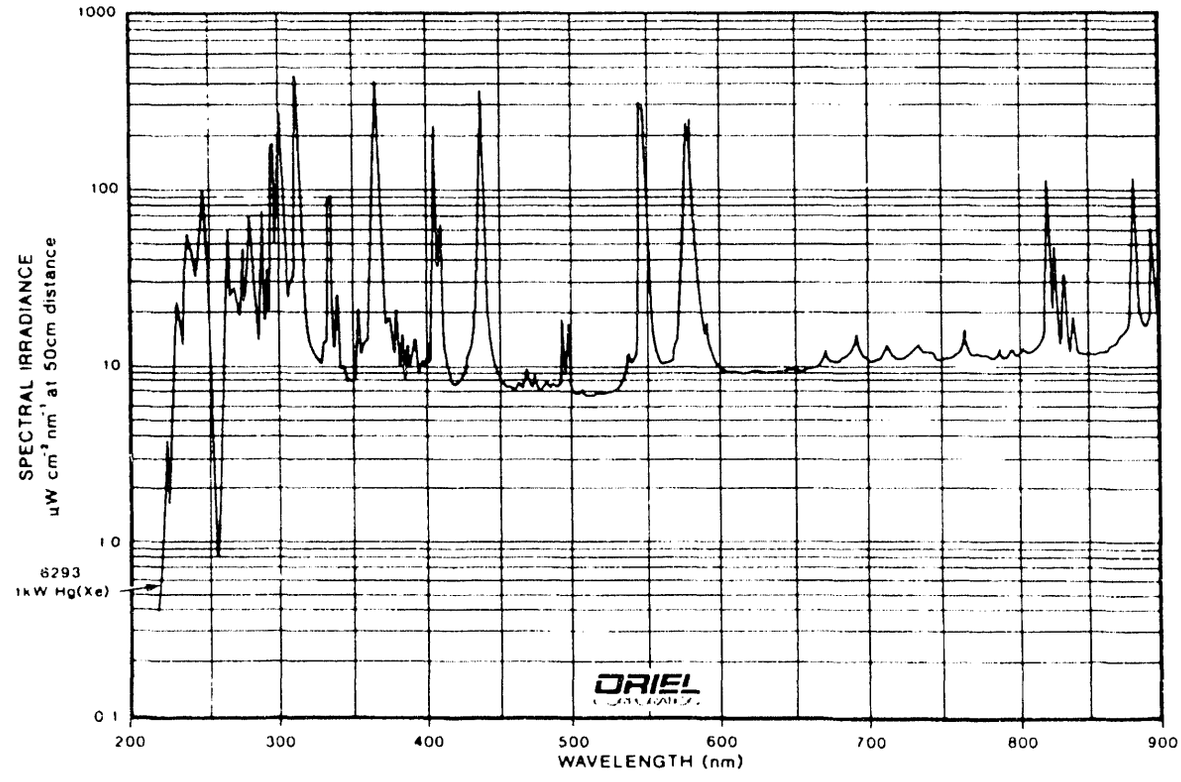

Fig. 10 - Spectral Irradiance of Hg/Xe (Mercury/Xenon) arc lamp [20]

Table 3 - Laser systems suitable for FMI excitation sources

Wavelength (nm)	Laser System	Pulsed or CW
190-1000+	Dye	pulsed
220-390	Frequency doubled dye	CW
325	HeCd	CW
330-380	Neon	CW
333-364	Argon Ion	CW
333.6	Argon	CW
337	Nitrogen	pulsed
345-500	Ti:Sapphire	pulsed
351	XeFl	pulsed
351.1	Argon	CW
351 or 355	Nd:glass	pulsed
365	Nd:YAG	pulsed

Pulsed systems, such as the dye lasers or solid state lasers, can be relatively inexpensive, but for FMI, two successive exposures (one for the cold image and one for the hot image) may contain different numbers of pulses from the laser. Although this may sound like a small problem, it adds another process that may reduce the temperature resolution of the system. Dye lasers do have the ability to be tuned over a broad range of wavelengths giving them an advantage when and if other fluorescent compounds are developed. For the system being developed at Sandia, a 15 mW HeCd laser system has been chosen because it is a small CW system that is relatively inexpensive. Other known systems use Hg arc lamps or pulsed dye lasers.

The next step for system design is to choose a camera system. Existing systems, without exception, use slow-scan CCD cameras. In this case, slow-scan refers to the frame rate at which data is read out of the CCD array. Television cameras adhere to the NTSC video standard where the CCD array in a CCD camera would be read at a rate of 30 frames per second. While this frame rate is good for television cameras, for quantitative analysis of the image content it is relatively poor. High quality TV cameras can approach 400 lines of information in about 500 fields with about 8-bits of dynamic range.

As we saw in the previous section, using a camera system with 8-bits of dynamic range would limit system sensitivity to roughly 0.4% change in quantum efficiency, or 1 part in 256. Slow-scan cameras are available with 12 to 16-bits of dynamic range and can thus image changes in intensity from 1 part in 4096 to 1 part in 65536 in an image of size ranging from 512 by 512 to 1024 by 1024 pixels. This translates into an order of magnitude gain in *possible* difference in temperature resolution.

Slow-scan cameras, since they do not adhere to TV standards, are designed to stare at a field of view and integrate for a variable length of time. For a situation where there is a very small amount of light being emitted, the camera can stare at the field of view for several minutes to several hours or until the detector becomes saturated. In contrast,

when using TV cameras for low light situations, it is necessary to grab and add video frames together, which also adds noise. Image averaging can be used to help remove noise, but it doesn't boost signal.

Noise in collected images is a second factor that will limit temperature resolution. Slow-scan cameras are almost always either peltier or liquid nitrogen cooled. Cooling helps to eliminate thermal generation of electron-hole pairs which can fill up CCD charge wells with noise instead of images signal. Peltier, or liquid/peltier, cooled systems generally operate at -39 °C or so and, as a result, generate only several electrons per second of noise with a well capacity of several hundred thousand electrons. Liquid nitrogen cooled systems, by cooling to a much lower temperature, keep the noise down to several electrons for every ten to one hundred seconds. With these systems, the readout electronics also add a small, but predictable amount of noise to the image, typically several electrons or tens of electrons per pixel. The noise qualities of these cameras and their integration capabilities, along with spectral sensitivities past 1 micron has prompted manufacturers of light emission systems to use them in lieu of TV cameras.

In general, virtually any camera which can yield an image in digital format, either directly or by frame grabbing, can be used for FMI. While TV cameras will work, they may become the limiting factor for thermal resolution. In applications where the technique is needed, but funds to build a system are scarce, TV cameras may be a good solution. However, the use of slow-scan CCD cameras will insure that the camera is not the limiting factor in system performance.

Lastly, the optical platform to house the excitation source and camera must be decided upon. In order to electrically bias the sample, probe stations provide an obvious choice for an FMI system. Most systems used for probing fine geometries have optics boxes that have TV camera ports. The most common optics assemblies are made by Bausch & Lomb and Mitutoyo. Since they are used during probing, the lenses on these systems are extra-long working distance, but have to sacrifice some optical quality.

Standard metallographic microscopes generally have superior optical systems, but suffer from short working distance objectives and limited facilities for electrical biasing of the sample. Most microscopes do have c-mount camera ports or other ways of attaching a camera.

Depending on the application, whether it is primarily packaged ICs or wafer level analysis, the optical platform that best suits the most frequent use of the system should be used.

Once the three main system components have been selected, the remaining considerations are relatively small. A computer with image processing capabilities that can handle the requirements outlined in the previous section is needed. The number of possibilities for this part of the system is too great to warrant much further discussion. It is sufficient to state that virtually any computer that you can get the image to will work without affecting performance, other than image processing speed, of course.

Traditional FMI systems input the excitation source through a UV grade fiber optic cable onto the sample at an oblique angle [4]. This does remove many headaches from the optical system, but tends to limit the amount of light that can be easily be sent to the sample, especially when using high magnification, shorter working distance lenses. Even on a probe station, a 50x lens will have a short enough working distance to complicate sample illumination. The use of a "through-the-lens" type of illumination removes the problems of sample illumination, but adds the problems encountered with non-UV transparent optics found in most microscopes. Generally, standard optical components offer transparency for light with wavelengths greater than about 370 nm. UV grade components are available because of the market for people doing fluorescence work, but the components, such as lenses, tend to be very limited in application and type, (e.g. magnification, working distance, numerical aperture, etc.).

The final system component needed is a custom interference filter to filter out all of the fluorescence except the dominant line at 612 nm as shown in Fig. 5. Most manufacturers of optics or filters will be able to put together a filter sandwich that can meet the requirements of FMI. A filter with a bandwidth of about 2 nm to 4 nm will be sufficient.

Now that we have discussed some of the system design considerations, it would be beneficial to describe some of the systems that have been assembled to do FMI.

First, in their original work, Kolodner and Tyson [4,5] describe what they felt would be a typical system for FMI. They did not provide details about the optical system, but they did use a probe station and mounted the slow-scan CCD camera with the interference filter in front, on the TV camera port. Their first CCD array was a 100 x 100 array but they later upgraded to a camera with a 384 x 576 array that was peltier cooled. They sent the light from a 100 watt Hg arc lamp through IR and blue-glass filters and a fiber optic cable and brought it to focus on the sample at an oblique angle. Image processing, remember that this is circa 1983, was done on a PDP 11/73 type computer. This system worked well enough that they could measure 0.01 °C thermal and 0.7 μm spatial resolution. The only systems that were known to be commercially marketed to FMI were virtually identical to this system, but benefited from some computer improvements. A system configured in this manner is illustrated in Fig. 11.

The system under development at Sandia represents a good contrast from the system just described. Sandia decided to implement the system on a Zeiss LSM (Laser Scan Microscope) and to illuminate the sample through the lenses using a 15 mW HeCd laser. The laser will be pumped through a UV grade fiber optic cable through some UV transparent objectives. This arrangement is illustrated in Fig. 12. The bulk of the problems that are being encountered at the time this writing are with the optics being virtually opaque to light at 325 nm. Nevertheless, there are UV objectives available from a third party that may be usable and the manufacturer of the microscope has ideas on how to pump the light to the objectives. Aside from this problem, system implementation is straightforward.

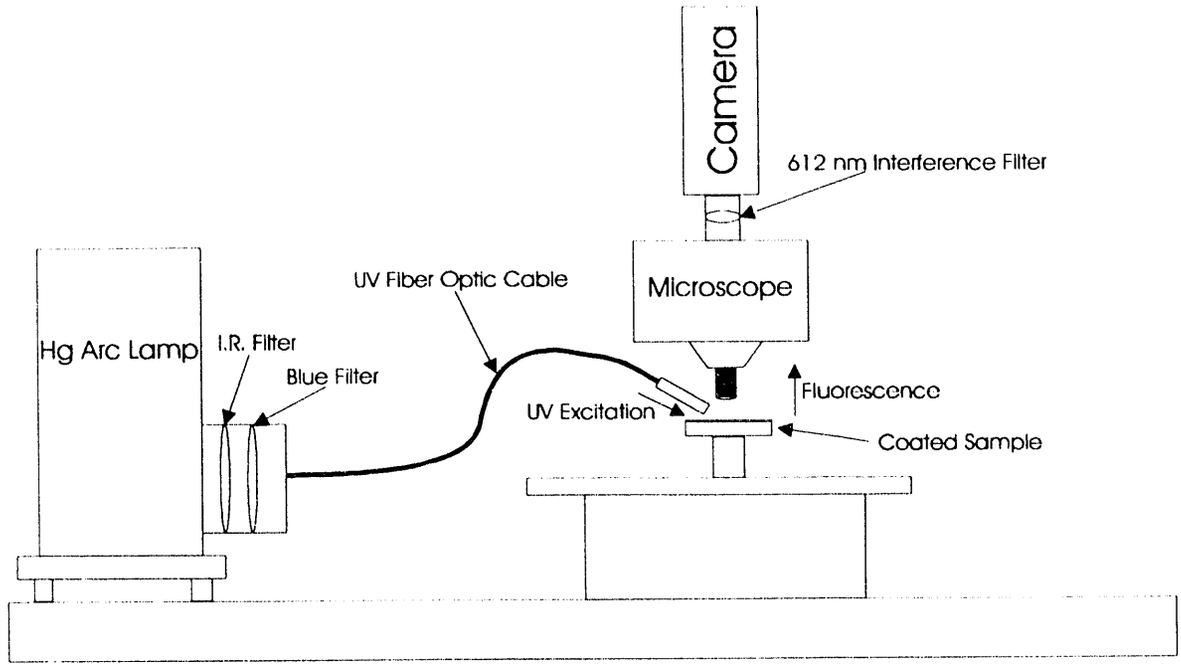

Fig. 11 - Implementation of FMI Using Hg Arc Lamp and Oblique Illumination

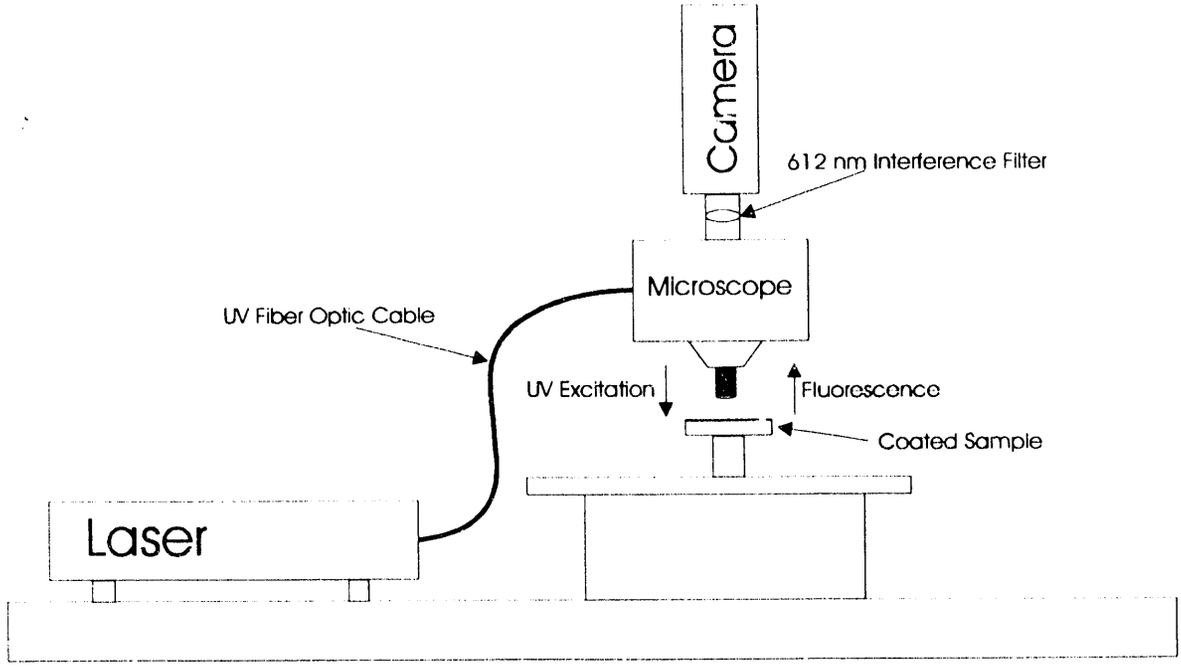

Fig. 12 - Implementation of FMI Using Laser and Coincident Illumination

A Photometrics slow-scan CCD camera was chosen that features a liquid/peltier cooling system and interfaced into a Sun workstation through a remote VME bus. The CCD array chosen was a Tektronics TK512 device with 512 by 512 pixels and charge wells averaging over 600,000 electrons. The deep wells allow us to use the full 16-bit dynamic range available as an option on the camera electronics. The array was also thinned and is back

illuminated to enhance the light collection efficiency. Larger arrays, such as the of 1024 by 1024 or 2048 by 2048 types are available, but they added significant cost and reduced the cell dimensions and thus the full well capacity. A photo of the system as of this writing is shown in Fig. 13. The figure shows the LSM with the Photometrics CCD camera mounted, the Sun workstation used to control both the microscope and the CCD camera, and barely visible is the HeCd laser to the right of the microscope. When complete, the microscope will be contained in a light tight, interlocked box for both the exclusion of stray light and for safety reasons.

The Sun computer platform was chosen so that the collected images could be directly imported into Khoros, an image processing software package written by the Khoros Group originally with the University of New Mexico [21]. Khoros has many more capabilities than will be needed by FMI, but its power for this application comes from being able to control both the LSM and the CCD camera directly through easy to make Khoros routines called glyphs. Once the control glyphs have been established, taking the series of images, and processing them into a thermal profile can be done through a single mouse click.

Example Applications:

In this final section, examples of past applications of the FMI technique to IC technology problems will be presented. In general, there will be some overlap with other possible techniques, such as light emission, where the location of the failing site could be found with a lot less trouble. There are also applications where excess current is drawn, and no light emission is observable; this is where high resolution thermal imaging is needed.

BiCMOS modeling example

The first example is a very straightforward application of FMI. An engineer was working on a new BiCMOS technology and had noticed that the simulated and measured I-V characteristics of the bipolar transistors did not match. He noticed that the mismatch was especially bad when the transistors began to draw several milliamps of current. His theory was that the transistor was heating up and since the simulations assumed a constant temperature, this created a difference. FMI was used to measure the temperature of the channel region of the transistors. It was found that even with only a milliamp or so of current, the transistor was being heated approx. 5 to 10 °C. This procedure was repeated for several different transistor layouts and for several current levels on each device. The

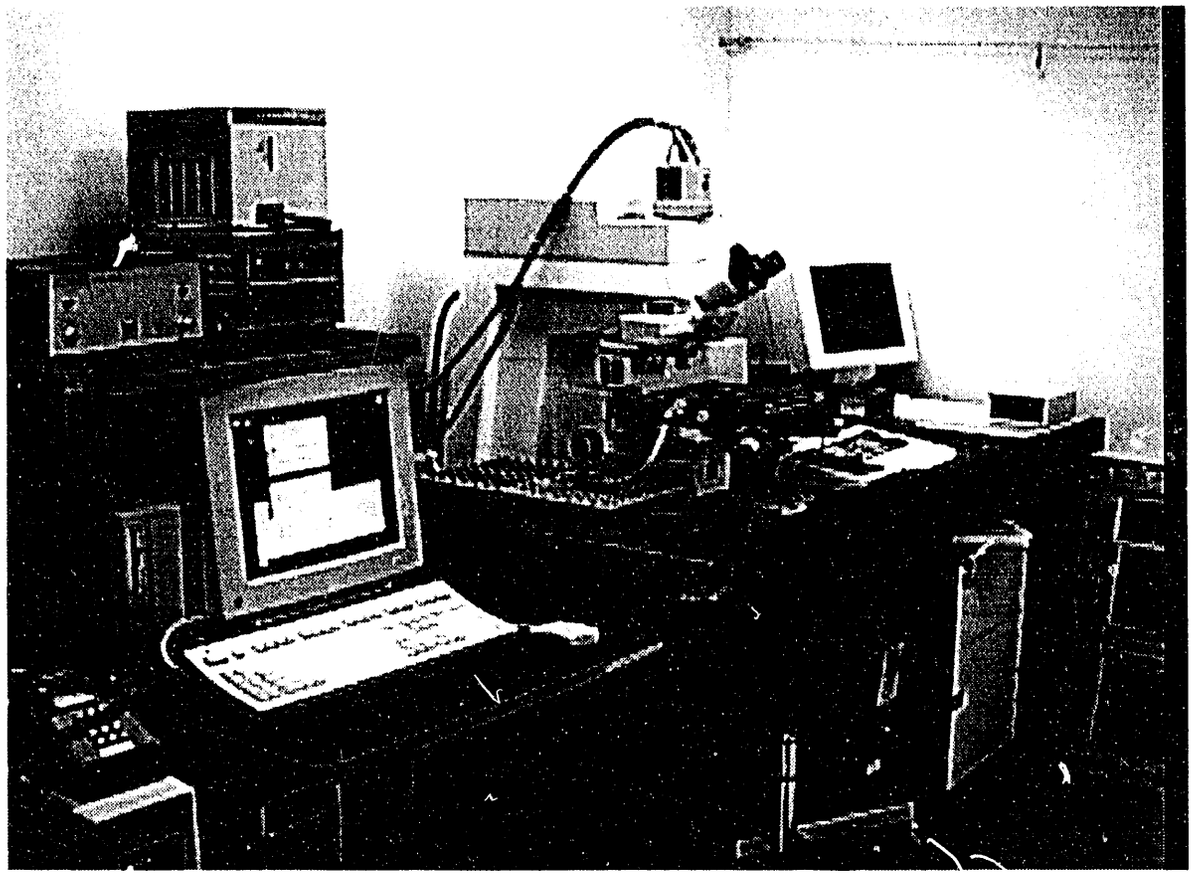

Fig. 13 - Implementation of FMI on Zeiss LSM using Photometrics CCD camera and LiCONIX UV laser

result, after incorporating temperature differences in the models, yielded an excellent agreement between measured and simulated results.

Fig. 14 shows, unfortunately, the only FMI example that I had available at this writing. This image came from an old system that had been used for thermal imaging. This was the only image saved from a hard drive that developed problems. The other examples to be discussed here would have had images to support the text had the drive not failed.

This example shows a bipolar transistor from the BiCMOS technology described above with several milliamps of current flowing through it. The vertical line coming from the top of the transistor measures approx. 2 μm. This line can act as a scale for observing the spatial resolution of the thermal image. The hottest zones in-between the fingers of the transistor, using the scale from the metal line, are demonstrating sub-micron resolution in an image where the temperature change is several degrees centigrade.

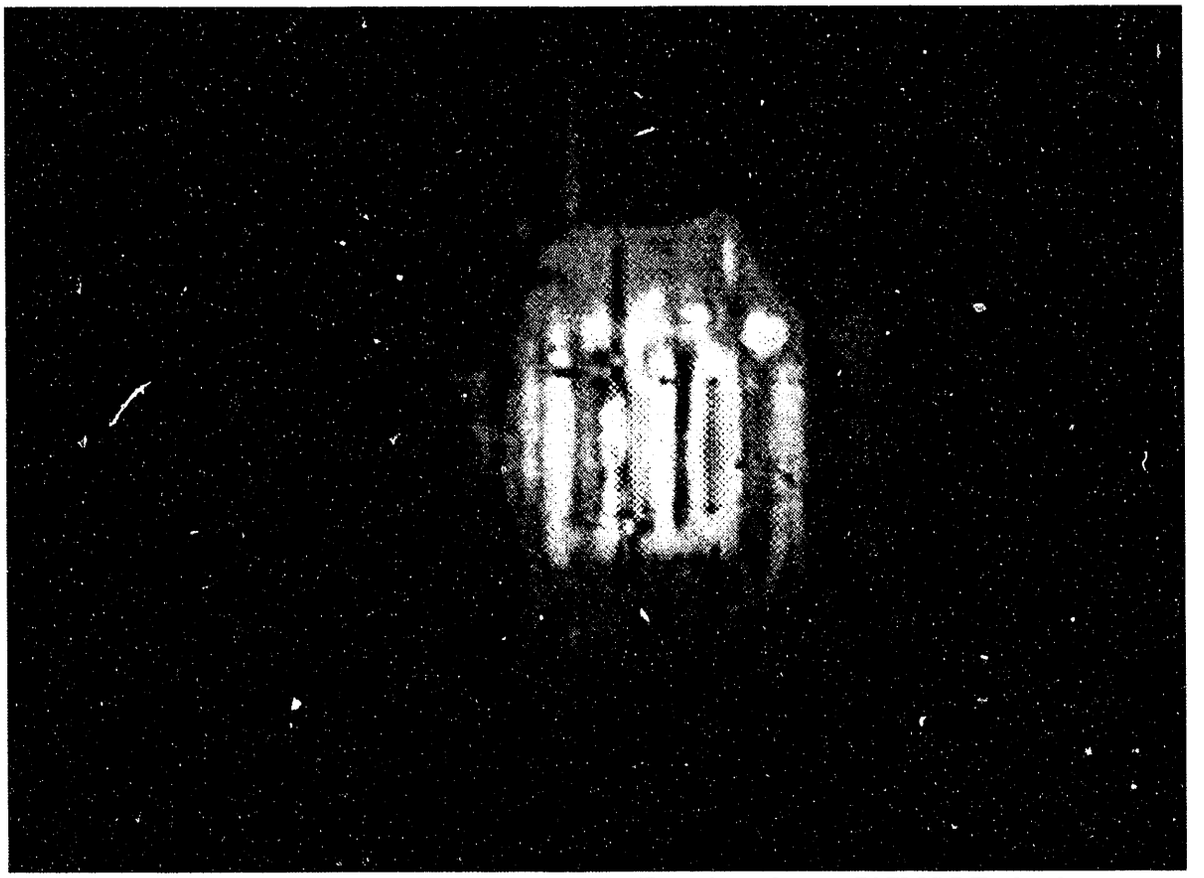

Fig. 14 - Fluorescent Microthermal Image of a Transistor from a BiCMOS Technology

Microprocessor latchup problem

Several samples from a microprocessor production lot suffering from a latchup problem, were submitted for failure analysis. The packages were opened on several of the ICs and FMI was used to study the surface temperature of the IC while the part was placed into latchup. In the thermal images, it was noted that the transistors on one side of a large p-well were latching up first, while transistors on the other side of the well did not go into latchup until much higher current levels were applied. After examining the layout for the IC, it was found that a single tub-tie was present on the large p-well. The transistor farthest away from the tub-tie latched up first and those closest to it did not latch before catastrophic damage had occurred. A new mask was generated to add several tub-ties at locations around the p-well, completely solving the latchup problem.

Electromigration test structure evaluation

Many companies have been interested in electromigration test structure design. In order to predict the stress on the structure, its temperature must be known. Usually, a uniform temperature is assumed. FMI has been used to study the temperature distribution of electromigration structures; specifically SWEAT type structures, both with and without underlying topography. FMI showed that there was a severe non-uniformity in the temperature distribution across the structure. Since the EuTTA film is not usable for thermal imaging at temperatures much above 60 °C, FMI could not be used to monitor the structure while being stressed to failure. FMI was able to look at the thermal

characteristics of the structure while a current was passed through it to heat it to around 50 °C.

SWEAT electromigration structures have traditionally been a single length of metal. In contrast, many conventional electromigration structures have been fabricated in a long meander layout. FMI analysis of meandering structures showed significant temperature non-uniformity between the center of the structure and the edges, with the center being significantly hotter than the edges.

Analysis of Zener diode turn-on characteristics
Another designer wanted to use FMI as a tool to understand the turn-on characteristics of zener diodes and investigate how differences in layout of the diode affected the turn-on characteristics. For this problem, FMI was able to identify the points in the diode that first turned on from the thermal signature. Structures ranging from squares and almost circles to trapezoids and rectangles were analyzed. The designer also looked at these structures using light emission and obtained similar results.

FA work on ESD damage to input structures
Traditionally ESD type failures on integrated circuits can be difficult to find. While their electrical signatures are easy to identify, the physical phenomenon causing the electrical response can be difficult to find. Usually, metal migration under the electrical stress creates a low resistance path in the input protection structure creating a leaky input characteristic. Light emission from a metal-to-metal short will be very small unless the structure is heated to high temperatures, i.e., passing a large current through the short. In contrast, FMI with its high thermal sensitivity, is ideal for this application. Many ESD failures have been analyzed using FMI.

In general, any situation where excess current may be flowing through a sample would be a good candidate for FMI analysis. There are a large number of failures that draw excess current, but do not emit light. Light emission, while a very powerful tool for IC failure analysis, cannot find all types of failures. A tool like FMI provides coverage for failure modes not detectable by other means. Since the application of FMI to an IC is non-destructive and easy to do, it is a tool that can be used without hesitation.

Conclusion

In this tutorial, the subject of microthermal imaging was reviewed fully. By introducing the physics that describes the spectral properties of heated bodies, the physical origins of the limitations of IR thermal techniques were studied. We found that the thermal resolution of IR systems can quite good for IC applications, but the spatial resolution is quickly becoming an order of magnitude too large. Fluorescent microthermal imaging (FMI) was originally invented to overcome the spatial resolution limitations imposed by imaging IR radiation. In its present form, FMI relies on light emitted by a fluorescing compound at 612 nm to achieve a spatial resolution of approximately 0.3 μm.

The study of FMI was broken down into its basic elements so that each area could be detailed properly. The technology behind the temperature-dependent fluorescing film was presented, followed by the image processing techniques needed to turn changes in quantum efficiency into changes in temperature. Once the theory behind FMI was covered, system hardware considerations were addressed. The multitude of possibilities of excitation sources and imaging hardware were covered in general to give readers an understanding of the tradeoffs involved when deciding upon a particular platform. Finally, some examples of applications of FMI were presented. At the time of this writing, the author's system is still under construction. As such, only a single image showing the capabilities of FMI could be included. Within the next few months, more examples will become available.

In closing, FMI is a technique that has been around for almost a decade, but has seen limited use throughout the microelectronics industry. One of the goals of this tutorial is to enlighten those not yet familiar with this technology to encourage more people to try FMI for themselves and learn what it can do for them.

Acknowledgments:

I would like to thank C. L. Henderson, J. M. Soden, and W. M. Miller for reviewing this manuscript. This work was performed at Sandia National Laboratories and is supported by the U.S. Department of Energy under contract DE-AC04-76DP00789.

References:

1. J. Hiatt, "A Method of Detecting Hot Spots on Semiconductors Using Liquid Crystals", *Proc. IRPS*, 1981, pp. 130-133.
2. G. D. Dixon, "Cholesteric Liquid Crystals in Non-Destructive Testing", *Materials Evaluation*, June 1977, pp. 51-55.
3. A. Geol, A. Gray, "Liquid Crystal Technique as a Failure Analysis Tool", *Proc. IRPS*, 1980, p. 115.
4. P. Kolodner, J. A. Tyson, "Microscopic fluorescent imaging of surface temperature profiles with 0.01 °C resolution", *Appl. Phys. Lett.* 40, 782 (1982).
5. P. Kolodner, J. A. Tyson, "Remote thermal imaging with 0.7 mm spatial resolution using temperature dependent fluorescent thin films", *Appl. Phys. Lett.* 42, 117 (1983).
6. R. Eisberg, R. Resnick, Quantum Physics, John Wiley and Sons, 1974, ch. 1.
7. E. Yang, Fundamentals of Semiconductor Devices, McGraw-Hill, 1978, ch. 6.
8. Barnes Infrared Radiometric Microscope Model RM-2A Instruction Manual
9. Barnes Infrared Micro Imager Model RM-50 Instruction Manual
10. C. T. Elliott, D. Day, D. J. Wilson, "An Integrating Detector for Serial Scan Thermal Imaging", *Infrared Physics*, Vol. 22, pp. 31-42, 1982.
11. D. Pote, G. Thome, T. Guthrie, "An Overview of Infrared Thermal Imaging Techniques in the Reliability and Failure Analysis of Power Transistors", *Proceedings of ISTFA*, pp. 63-75, 1988.

12. G. J. Zissis, Infrared Technology Fundamentals, *Optical Engineering*, Vol. 15, no. 6, pp. 484-497, 1976.
13. E. Hecht, A. Zajac, Optics, Addison Wesley, 1974, ch. 10.
14. P. Burgraaf, IR Imaging: Microscopy and Thermography, *Semiconductor International*, pp. 58-65, July, 1986.
15. H. Winston, O. J. Marsh, C. K. Suzuki, C. L. Telk, "Fluorescence of Europium Thenoylfrifluoroacetonate. I. Evaluation of Laser Threshold Parameters", *J. Chem. Phys.*, vol. 39, no. 2, pp. 267-270, July, 1963.
16. M. Bhaumik, "Quenching and Temperature Dependence of Fluorescence in Rare-Earth Chelates", *J. Chem. Phys.*, Vol. 40, (3711), 1964.
17. G. Crosby, R. Whan, R. Alire, "Intramolecular Energy Transfer in Rare Earth Chelates. Role of the Triplet State", *J. Chem. Phys.*, Vol. 34, (743), 1961.
18. E. Bowen, J. Sahu, "The Effect of Temperature on fluorescence of Solutions", *J. Phys. Chem.*, Vol. 63 (4), 1959.
19. P. Kolodner, A. Katzir, N. Hartsough, "Noncontact surface temperature measurement during reactive-ion etching using fluorescent polymer films", *Appl. Phys. Lett.* 42 (8), 15 April 1983.
20. Oriel Corporation, Light Sources, Monochromators, and Detection Systems catalog 1989, p. 85.
21. The Khoros Group, "Image Processing with Khoros", The University of New Mexico, 1992.

Appendix A

MATERIAL SAFETY DATA SHEET

EASTMAN KODAK COMPANY
343 State Street
Rochester, New York 14650

For Emergency Health, Safety, and Environmental Information, call 716-722-5151
For other purposes, call 800-225-5352 (in New York State call 716-458-4014)

Date of Preparation: 04/10/86 Kodak Accession Number: 908990

SECTION I. IDENTIFICATION

- Product Name: Europium(III), Thenoyltrifluoroacetonate
- Synonym(s):
  Tris(4,4,4-trifluoro-1-(2-thienyl)-1,3-butanedione)europium
- Formula: C24 H12 Eu F9 O6 S3
- CAT No(s): 130 4898; 130 5499
- Chem. No(s): 08990
- Kodak's Internal Hazard Rating Codes: R: U S: U F: 1 C: 0

SECTION II. PRODUCT AND COMPONENT HAZARD DATA

COMPONENT(S):	Percent	TLV(R)	CAS Reg. No.
Europium(III) Thenoyltrifluoroacetonate	approx 100	---	14054-87-6

SECTION III. PHYSICAL DATA

- Appearance: Yellow crystalline solid
- Melting Point: Not Available
- Vapor Pressure: Negligible
- Evaporation Rate (n-butyl acetate = 1): Negligible
- Volatile Fraction by Weight: Negligible
- Specific Gravity (H2O = 1): Not Available
- Solubility in Water (by Weight): Not Available

SECTION IV. FIRE AND EXPLOSION HAZARD DATA

- Flash Point: Not Applicable
- Extinguishing Media: Water spray; Dry chemical; CO2
- Special Fire Fighting Procedures: Wear self-contained breathing apparatus and protective clothing.
- Unusual Fire and Explosion Hazards: Fire or excessive heat may produce hazardous decomposition products. This material in sufficient quantity and reduced particle size is capable of creating a dust explosion.

SECTION V. REACTIVITY DATA

- Stability: Stable
- Incompatibility: Strong oxidizers
- Hazardous Decomposition Products: Combustion will produce CO2 and probably CO. Hydrogen fluoride gas and oxides of sulfur may also be present.
- Hazardous Polymerization: Will not occur.

SECTION VI. TOXICITY AND HEALTH HAZARD DATA

A. EXPOSURE LIMITS: Not established.

B. EXPOSURE EFFECTS:
The toxicological properties of this material have not been investigated. Exercise appropriate procedures to prevent opportunities for direct contact with the skin or eyes or to prevent inhalation.

C. FIRST AID:
Inhalation: Remove to fresh air. Treat symptomatically. If symptoms are present get medical attention.
Skin: Immediately flush skin with plenty of water for at least 15 minutes. Get medical attention if symptoms are present after washing.
Eye: Immediately flush eyes with plenty of water for at least 15 minutes and get medical attention.
Ingestion: Drink 1-2 glasses of water or milk. Call a physician.

SECTION VII. VENTILATION AND PERSONAL PROTECTION

A. VENTILATION:
Good general room ventilation should be used.
Local exhaust may be needed.

B. RESPIRATORY PROTECTION:
A NIOSH approved dust respirator should be worn if needed.

C. SKIN AND EYE PROTECTION:
Protective gloves and safety glasses should be worn.

SECTION VIII. SPECIAL STORAGE AND HANDLING PRECAUTIONS

Keep from contact with oxidizing materials.

SECTION IX. SPILL, LEAK, AND DISPOSAL PROCEDURES

Sweep up material and package for safe feed to an incinerator. Dispose by incineration or contract with licensed chemical waste disposal agency. Discharge, treatment, or disposal may be subject to federal, state or local laws.

For transportation information regarding this product, please phone the Eastman Kodak Distribution Center nearest you: Rochester, NY (716) 254-1300; Oak Brook, IL (312) 654-5300; Chamblee, GA (404) 455-0123; Dallas, TX (214) 241-1611; Whittier, CA (213) 945-1255; Honolulu, HI (808) 833-1661.

The information contained herein is furnished without warranty of any kind. Users should consider these data only as a supplement to other information gathered by them and must make independent determinations of the suitability and completeness of information from all sources to assure proper use and disposal of these materials and the safety and health of employees and customers.

END

DATE FILMED

11/23/93